

DTIC FILE COPY

RADC-TR-90-61
Final Technical Report
May 1990



PHASE TECHNIQUES FOR IMAGING AND RECOGNITION

Tufts University

Robert A. Gonsalves

AD-A226 233



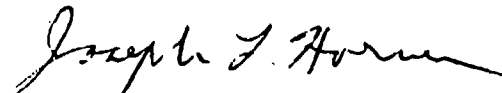
APPROVED FOR PUBLIC RELEASE; DISTRIBUTION UNLIMITED.

Rome Air Development Center
Air Force Systems Command
Griffiss Air Force Base, NY 13441-5700

This report has been reviewed by the RADC Public Affairs Division (PA) and is releasable to the National Technical Information Service (NTIS). At NTIS it will be releasable to the general public, including foreign nations.

RADC-TR-90-61 has been reviewed and is approved for publication.

APPROVED:



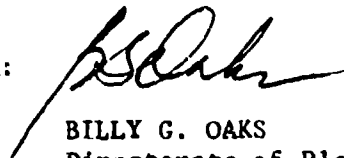
JOSEPH L. HORNER
Project Engineer

APPROVED:



HAROLD ROTH
Director of Solid State Sciences

FOR THE COMMANDER:



BILLY G. OAKS
Directorate of Plans & Programs

If your address has changed or if you wish to be removed from the RADC mailing list, or if the addressee is no longer employed by your organization, please notify RADC (ESOP) Hanscom AFB MA 01731-5000. This will assist us in maintaining a current mailing list.

Do not return copies of this report unless contractual obligations or notices on a specific document require that it be returned.

REPORT DOCUMENTATION PAGE			Form Approved CPM No. 0704-C188	
<small>Public reporting burden for this collection of information is estimated to average 1 hour per response, including the time for reviewing instructions, searching existing data sources, gathering and maintaining the data needed, and reviewing the collection of information. Send comments regarding this burden estimate or any other aspect of this collection of information, including suggestions for reducing this burden, to Washington Headquarters Services, Directorate for Information Operations and Reports, 1215 Jefferson Davis Highway, Suite 1204, Arlington, VA 22202-4302, and to the Office of Information and Regulatory Affairs, Office of Management and Budget, Washington, DC 20503.</small>				
1. AGENCY USE ONLY (Leave Blank)		2. REPORT DATE May 1990		3. REPORT TYPE AND DATES COVERED Final Jul 88 to Sep 89
4. TITLE AND SUBTITLE PHASE TECHNIQUES FOR IMAGING AND RECOGNITION			5. FUNDING NUMBERS C - F30602-88-D-0027 PE - 61102F PR - 2305 TA - J7 WU - P2	
6. AUTHOR(S) Robert A. Gonsalves				
7. PERFORMING ORGANIZATION NAME(S) AND ADDRESS(ES) Tufts University Electro-Optics Technology Center Medford MA 02155			8. PERFORMING ORGANIZATION REPORT NUMBER N/A	
9. SPONSORING/MONITORING AGENCY NAME(S) AND ADDRESS(ES) Rome Air Development Center (ESOP) Hanscom AFB MA 01731-5000			10. SPONSORING/MONITORING AGENCY REPORT NUMBER RADC-TR-90-61	
11. SUPPLEMENTARY NOTES RADC Project Engineer: Joseph L. Horner/ESOP/(617) 377-3841				
12a. DISTRIBUTION/AVAILABILITY STATEMENT Approved for public release; distribution unlimited.			12b. DISTRIBUTION CODE	
13. ABSTRACT (Maximum 200 words) Research is described on two aspects of phase manipulation in optical processing. Phase diversity uses multiple observations of an image, where the optical system is changed in a known fashion between observations. The images are processed to remove the effects of unknown phase degradations. We also study binary phase-only filtering and find that the binarization can be done in a phase-rotated space which gives rise to improved object recognition. One dimensional example of both techniques are given.				
14. SUBJECT TERMS Phase Retrieval Holography			15. NUMBER OF PAGES 56	
Phase-Only Filtering Optical Signal Processing			16. PRICE CODE	
17. SECURITY CLASSIFICATION OF REPORT UNCLASSIFIED	18. SECURITY CLASSIFICATION OF THIS PAGE UNCLASSIFIED	19. SECURITY CLASSIFICATION OF ABSTRACT UNCLASSIFIED	20. LIMITATION OF ABSTRACT UL	

ACKNOWLEDGMENT

The support of the Optical Processing Group, RADC, at Hanscom AFB is gratefully acknowledged. The author and his students, Joe Robichaud and John Hogan, had several stimulating discussions with Dr. Joseph Horner, whose support and encouragement was particularly valuable.



Accession For	
NTIS GRA&I	<input checked="" type="checkbox"/>
DTIC TAB	<input type="checkbox"/>
Unannounced	<input type="checkbox"/>
Justification	
By _____	
Distribution/	
Availability Codes	
Dist	Avail and/or Special
A-1	

Table of Contents

	Page
1. Introduction	1
2. Phase Diversity Imaging	2
2.1 General	2
2.2 The Mathematics of Phase Diversity	5
2.3 Examples	10
2.4 Details of the Search	17
2.5 Discussion	21
3. Recognition	22
3.1 General	22
3.2 Optical Processing	24
3.3 Examples	28
3.4 Phase Rotation	32
3.5 Discussion	44
References	45

Phase Techniques for Imaging and Recognition

1. Introduction

This report describes the use of phase in imaging systems and in recognition systems. The work was sponsored by RADC through a subcontract to Syracuse University and was conducted in the time period of July 1988 to July 1989.

The imaging application is to combat the deleterious effects of a turbulent atmosphere or a misaligned optical system. We describe the theory and give one-dimensional examples for a technique called "phase diversity". It uses a simple optical system to capture distorted images of an object and uses a computer algorithm to restore the image.

The recognition application uses phase-only filtering techniques to extract an object from a scene. We describe the math and give some one-D examples. We present anecdotal evidence that, if a binary phase-only filter is rotated in spatial frequency before it is binarized, an object is detected more efficiently in a scene. A metric to describe the efficiency is defined and an average-over-rotation technique is introduced.

2. Phase Diversity Imaging.

2.1 General

Many factors contribute to the distortion of a measured image. Two prime examples are (a) the turbulent atmosphere between the object and the imaging system, and (b) physical perturbations that degrade the optical system's point spread function.

Both of these effects are adequately modeled by a wavefront distortion (or phase aberration) $w(x,y)$ across the entrance pupil of the taking system. See Figure 1. This wavefront varies as a function of time and causes a distant point to spread and to dance across the image plane such that the image, integrated over the exposure time, is severely blurred.

One way to combat these distortions is to construct an adaptive optical system. By one means or another the wavefront is measured and a set of control signals is developed to push and pull a reflective, flexible membrane or a set of segmented mirrors that are placed in the optical path. These corrections attempt to introduce the conjugate wavefront $-w(x,y)$ so that the blurring is removed. Phase retrieval [1] is one way to measure the wavefront.

Wavefront sensing by phase retrieval implies extraction of the Fourier transform of a complex signal based on observation of the modulus of the signal. Only the image intensity from a

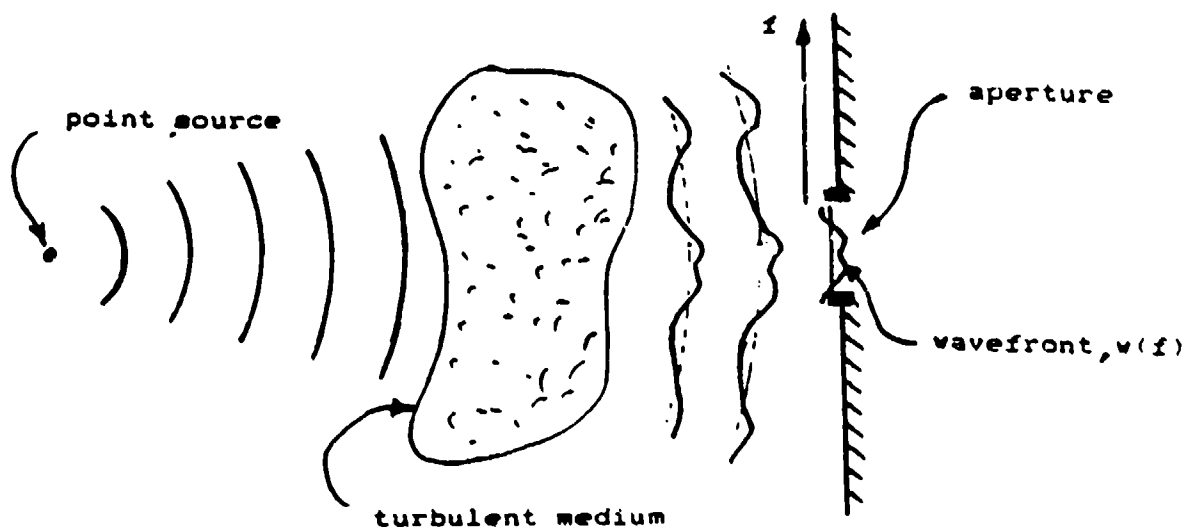


Figure 1. Generation of the wavefront $w(f)$.

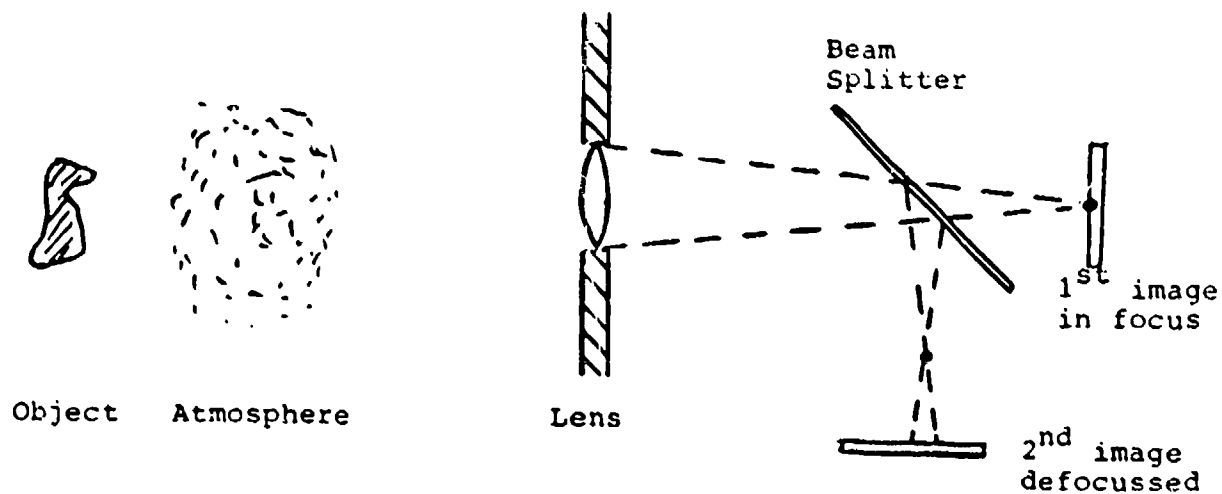


Figure 2. Quadratic phase diversity introduced with a beam splitter and two focal planes.

system's focal plane array is required to estimate the phase aberrations. These estimates are used to derive control signals to align (or to maintain alignment of) the optical system.

The phase retrieval concept can be used in both a predetection and post-detection mode. In the former, the control system labors to keep the optics in a diffraction-limited mode all the time. In the latter, the control system induces a phase diversity that allows successive images to be restored to nearly diffraction-limited quality by post-processing of the image. This second mode is particularly interesting because it will reduce the design effort for both the optical system and the control system.

A further advantage of this second mode, which we call "phase diversity," is that it can be used while the optical system is imaging an extended object. No separate point source (target "glint") or active imaging is needed. It is an entirely passive operation. The technique is described in detail in [2] and further results and examples appear in [3], where the technique is used to align an optical system.

A particularly simple kind of diversity is a quadratic phase. This can be introduced by defocusing the optical system. Thus, an in-focus image is measured and an out-of-focus image, one with quadratic phase diversity, is also measured, perhaps simultaneously, as shown in Figure 2.

2.2 The Mathematics of Phase Diversity.

With a distorting wavefront $w(f)$ across the aperture of an otherwise perfect optical system, the image of distant point source is

$$p(x) = |h(x)|^2, \quad (1)$$

where $h(x)$ has Fourier transform

$$H(f) = A(f) \exp(-j w(f)) \quad (2)$$

and where $A(f)$ is the aperture function. Figure 3 shows an unobscured aperture function $A(f)$ and the resulting $p(x)$'s for $w(f) = 0$ and for another, non zero $w(f)$.

If a distant, incoherent object $o(x)$ is imaged by an optical system with phase diversity, the observed images are

$$y_1(x) = o(x) * p_1(x) \quad (3)$$

$$\text{and } y_2(x) = o(x) * p_2(x) \quad (4)$$

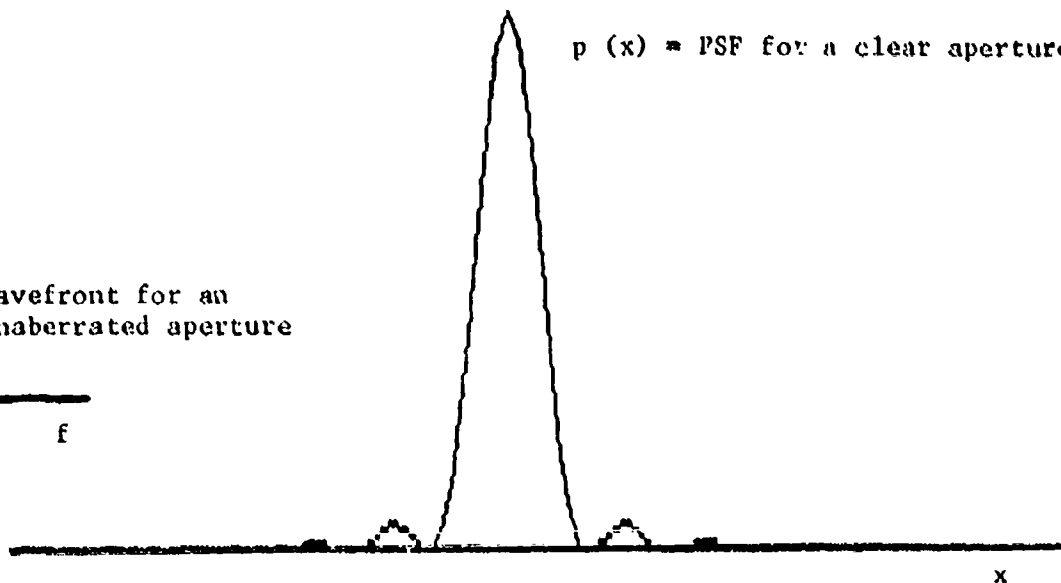
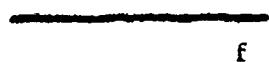
Both $y_1(x)$ and $y_2(x)$ (or their Fourier transforms $Y_1(f)$ and $Y_2(f)$) are observed. But neither $p_1(x)$ nor $p_2(x)$ is known. We know only that $p_2(x)$ is formed by adding a known phase diversity, usually quadratic, to the unknown wavefront $w(f)$.

$A(f)$ = aperture function



$p(x)$ = PSF for a clear aperture

$w(f)$ = wavefront for an unaberrated aperture



$w(f)$



$p(x)$ = PSF for an aberrated aperture

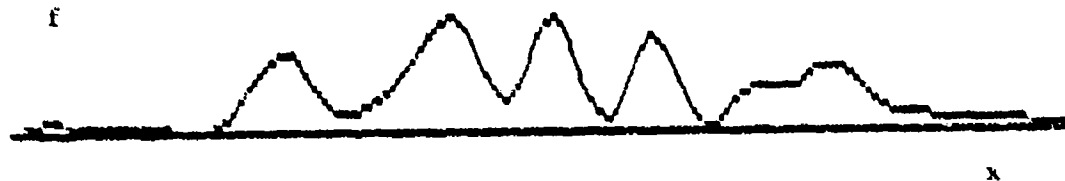


Figure 3. Point spread functions for a clear and an aberrated aperture.

If, however, we are able to estimate $P_1(f)$ and $P_2(f)$, a reasonable estimate for $O(f)$ is [1]

$$\hat{O}(f) = \frac{Y_1(f) \hat{P}_1^*(f) + Y_2(f) \hat{P}_2^*(f)}{|\hat{P}_1(f)|^2 + |\hat{P}_2(f)|^2}, \quad (5)$$

where $\hat{P}_1(f)$, $\hat{P}_2(f)$ and $\hat{O}(f)$ are the estimates of $P_1(f)$, $P_2(f)$ and $O(f)$, respectively. We are left with the problem of estimating $P_1(f)$ and $P_2(f)$.

Also in Reference [1], Gonsalves suggests a metric for estimating $P_1(f)$ and $P_2(f)$. The metric is

$$E = \int [Y_1(x) - g_1(x)]^2 dx + \int [Y_2(x) - g_2(x)]^2 dx, \quad (6)$$

where $g_1(x) = \hat{O}(x) * \hat{p}_1(x)$ or $G_1(f) = \hat{O}(f) \hat{P}_1(f)$ (7)

and $g_2(x) = \hat{O}(x) * \hat{p}_2(x)$ or $G_2(f) = \hat{O}(f) \hat{P}_2(f)$. (8)

That is, one forms joint estimates for $o(x)$, $p_1(x)$ and $p_2(x)$; then (7) and (8) are used to find an estimate for the two observed signals $y_1(x)$ and $y_2(x)$, namely $g_1(x)$ and $g_2(x)$; then the mean square error is calculated as in Equation (6).

The procedure reduces to a curve fitting exercise. One estimates the wavefront as $\hat{w}(f)$ and, from Equations (1) and (2), the estimated point spread function $\hat{p}_1(x)$. Then one adds the known phase diversity to $\hat{w}(f)$ and calculates $\hat{p}_2(x)$. Next the object's estimated Fourier transform is calculated from Equation

(5). And, finally, the mean square error metric E is calculated from Equation (6).

A search procedure is used to modify the estimated wavefront $\hat{w}(f)$ until E is a minimum. The procedure yields estimates of both the unknown wavefront and the unknown object.

Reference [1] also shows that Equations (5), (7) and (8) can be used to simplify the calculation of the metric E . Thus, (6) becomes

$$E = \int \frac{|Y_1(f) \hat{P}_1(f) - Y_2(f) \hat{P}_2(f)|^2}{|\hat{P}_1(x)|^2 + |\hat{P}_2(f)|^2} df. \quad (9)$$

This means that E can be calculated without actually calculating the object spectrum $\hat{O}(f)$.

A block diagram of the procedure is shown in Figure 4. Examples are given in the next subsection.

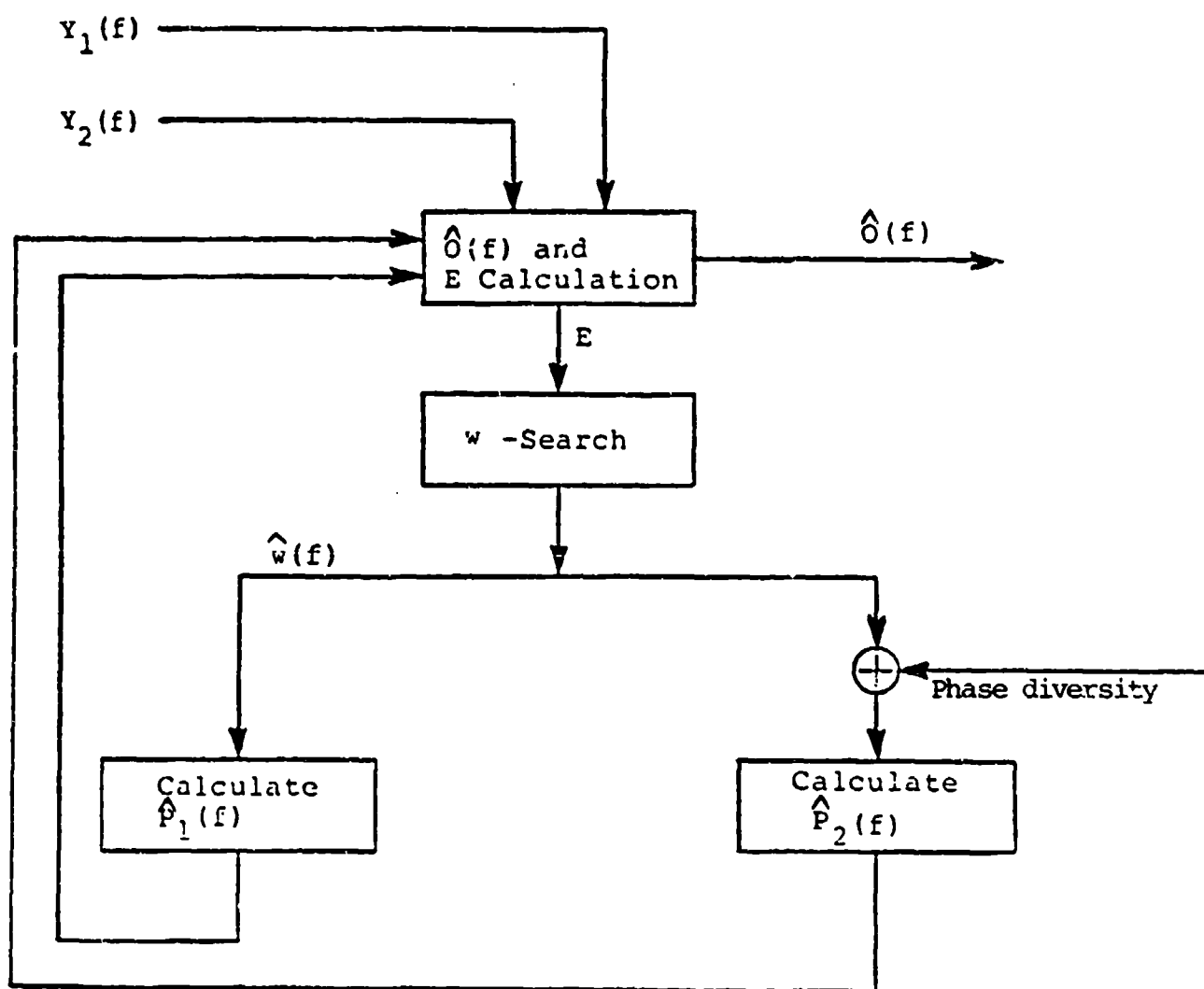


Figure 4: Estimation of $w(f)$ and the object spectrum

2.3 Examples.

In Figure 5 we show phase aberrations with and without diversity. The upper phase, $w_1(f)$, contains both quadratic and cubic terms in f . The lower phase, $w_2(f)$, has a quadratic phase term added to $w_1(f)$ so the wavefront $w_2(f)$ contains more waves of aberration. Figure 6 shows the input object and the two point spread functions, $p_1(x)$ and $p_2(x)$. Figure 7 shows the two observed images $y_1(x)$ and $y_2(x)$. We used these two to make an estimate of both $w(f)$ and the object. The estimate, $\hat{o}(x)$, shown in Figure 7 is a nearly perfect version of the input object.

This example is ideal in two respects. There is no noise added to the observations and the unknown wavefront $w_1(f)$ has only two degrees of freedom: focus and coma. The search routine has no problem finding $w_1(f)$.

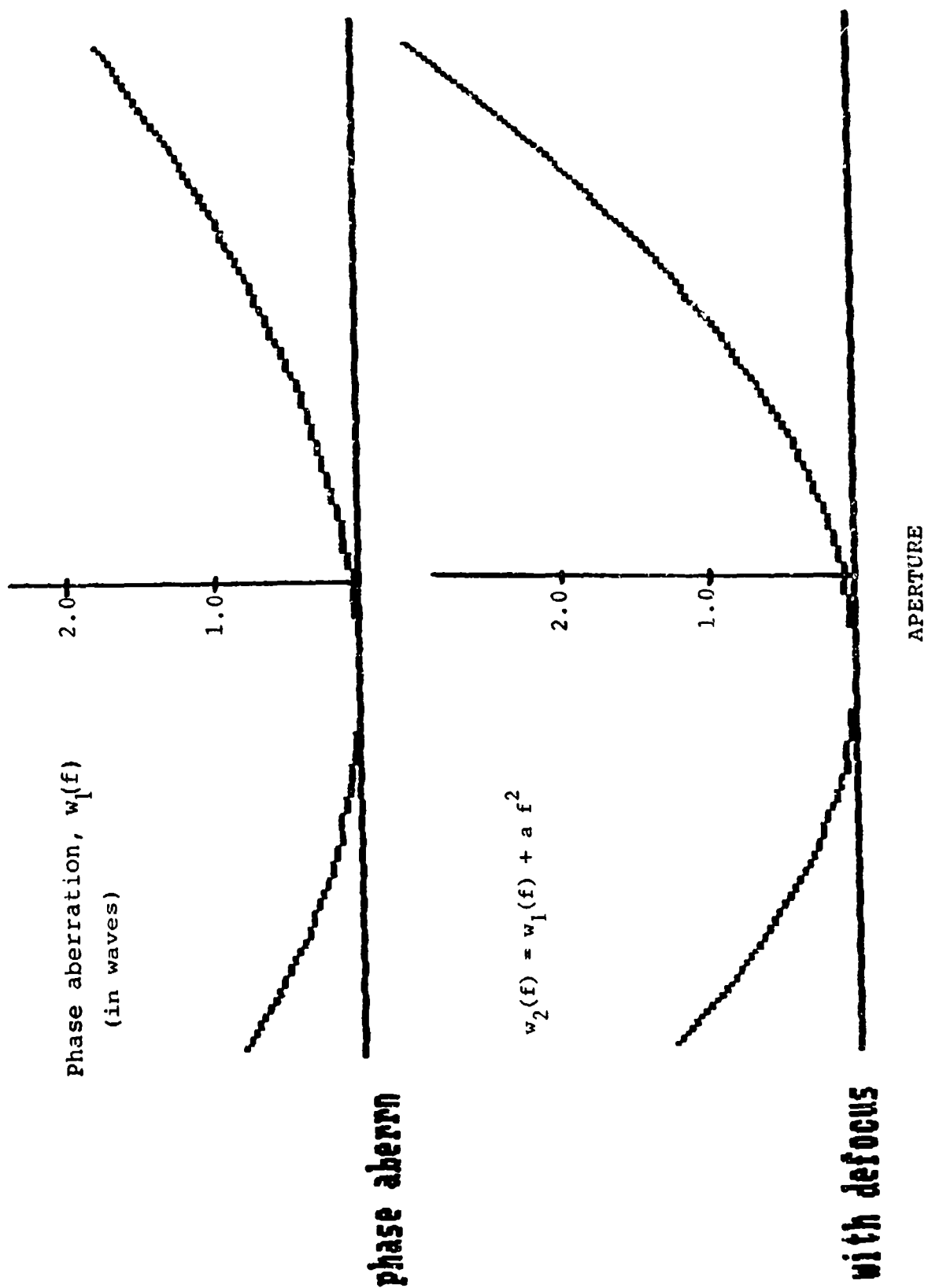


Figure 5. Phase aberration with and without defocus.

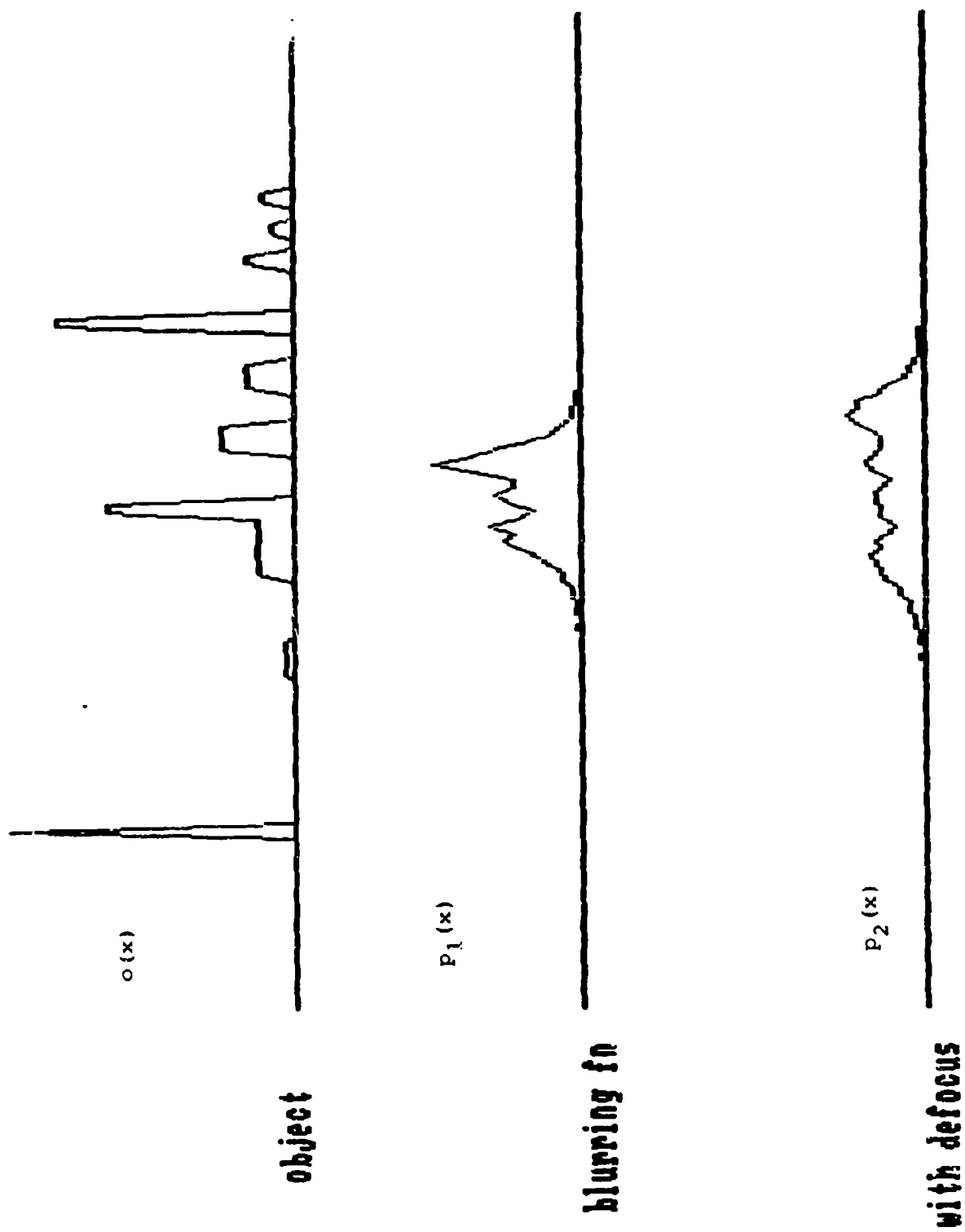


Figure 6. Input object; and first and second point spread functions.

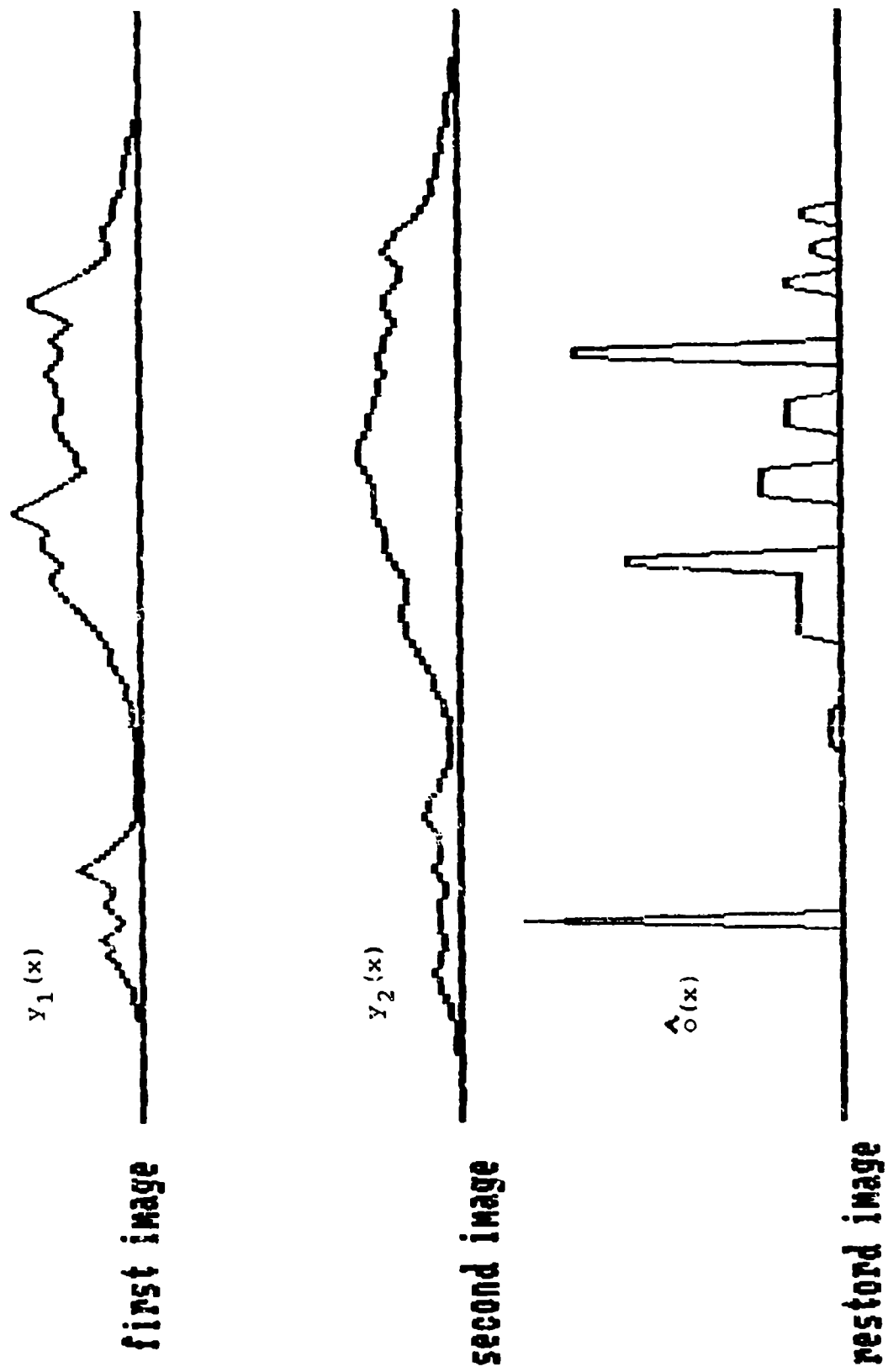


Figure 7. First and second observed images; and the restored image.

When noise is added the results are, typically, as shown in Figures 8 and 9. In Figure 8 noise of rms value 3.0 is added to data with a maximum value of 120 for a signal-to-noise ratio of 40.0. This result was calculated with the exact $w_1(f)$, as if it were known. It shows the effect of noise on signal estimation.

In Figure 9 we show a typical result when $w_1(f)$ must be estimated based on the noisy data. The estimation procedure yields a $w_1(f)$ which is only slightly inaccurate (focus = 0.166 instead of 0.170 and coma = 0.000798 instead of 0.000800 and the estimate of the object suffers very little. Figure 9 shows how well the object can be estimated when $w(f)$ and the object must be estimated, jointly, at least for simulated data.

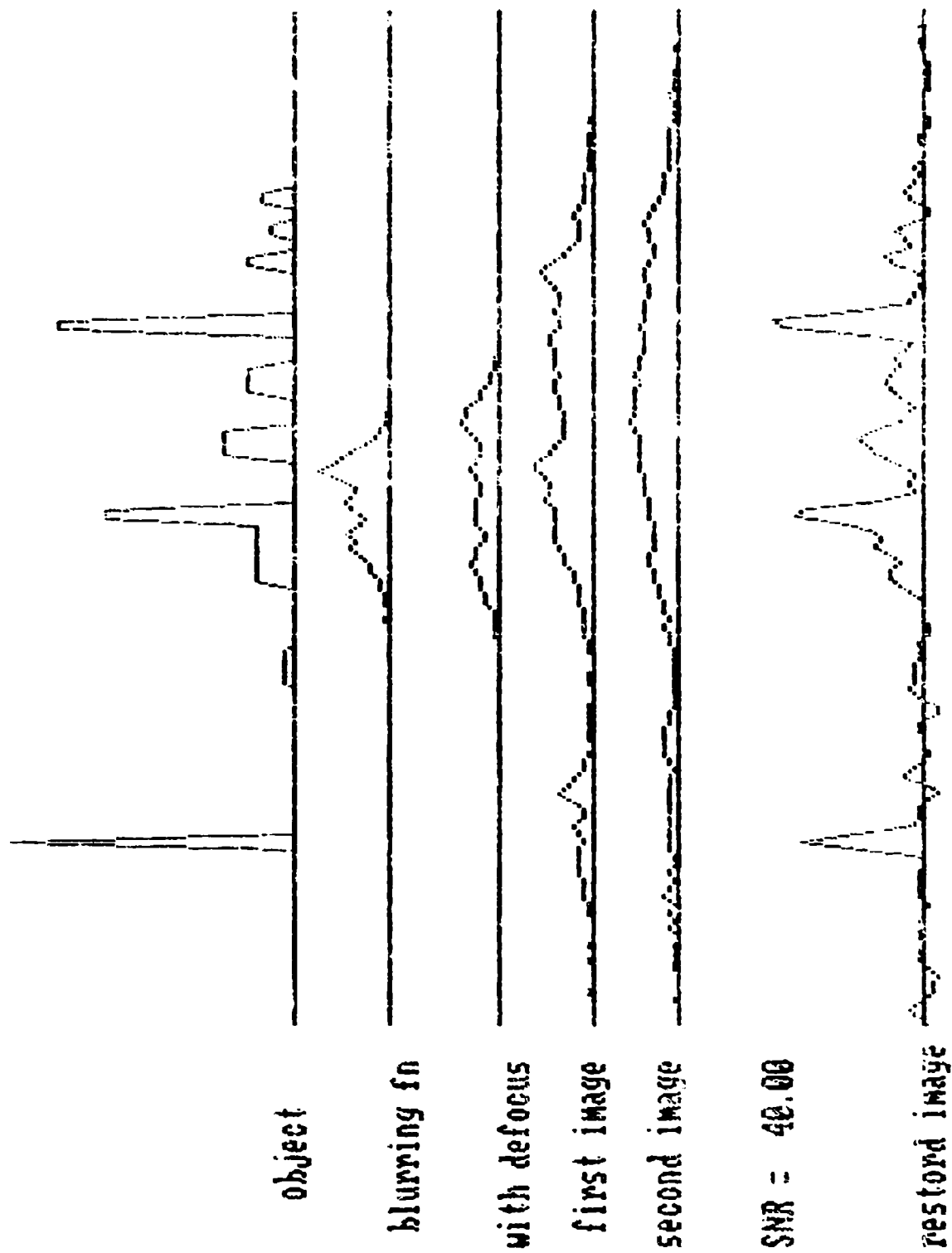


Figure 8. Phase diversity imaging with noise, known $w_1(f)$.

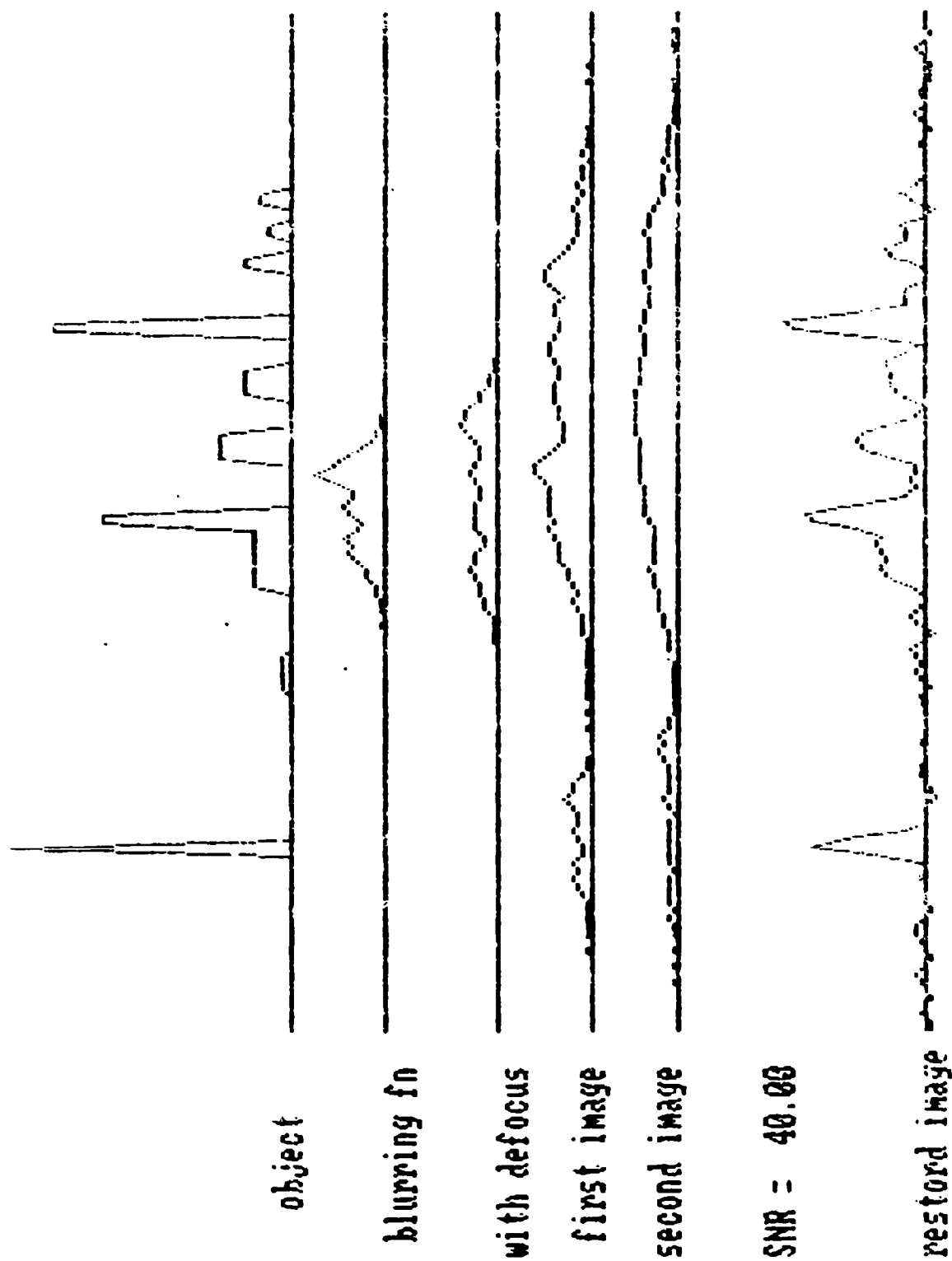


Figure 9. Phase diversity imaging with noise, unknown $w_1(f)$.

2.4 Details of the Search.

In Figures 10, 11 and 12 we show some details of the search for focus and coma in $w_1(f)$. Figure 10 shows the metric as the parameters vary over a region around the true values. The minimum is quite broadly defined.

Figure 11 shows the actual search path in focus-coma space. Many (18) iterations of a one-dimensional search, alternating in focus and coma, were used to find the minimum mean square error.

Figure 12 shows how the metric varies when coma is held constant and when focus is held constant. The curves show that the metric has, indeed, a well-defined minimum.

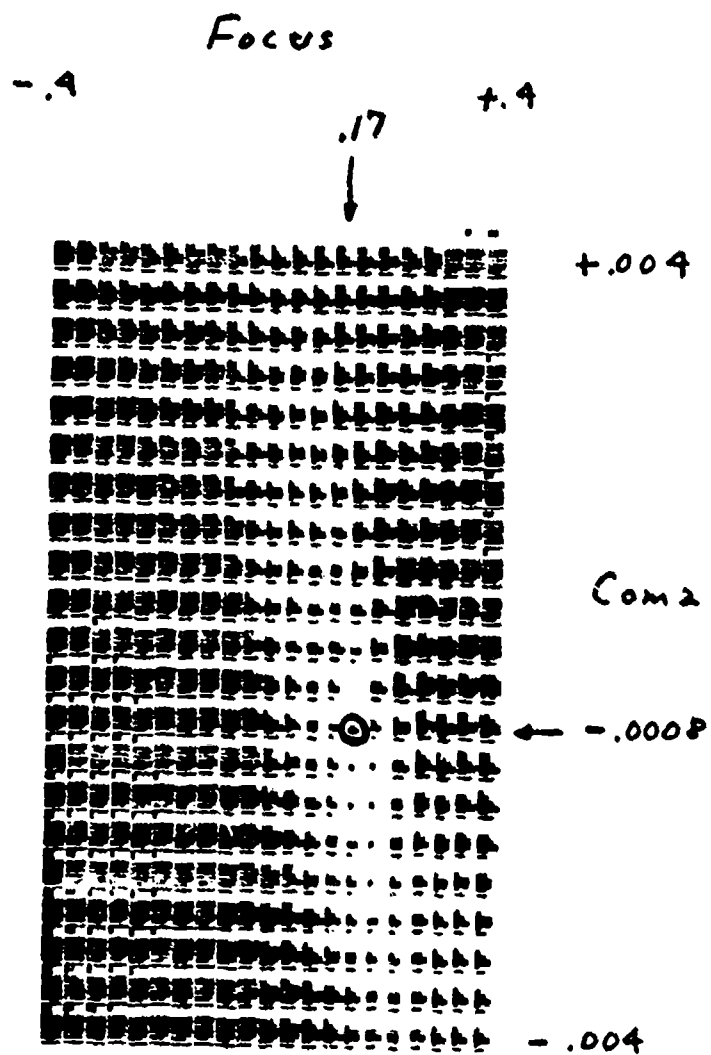


Figure 10. MSE search metric vs. focus and coma.

SEARCH PATH

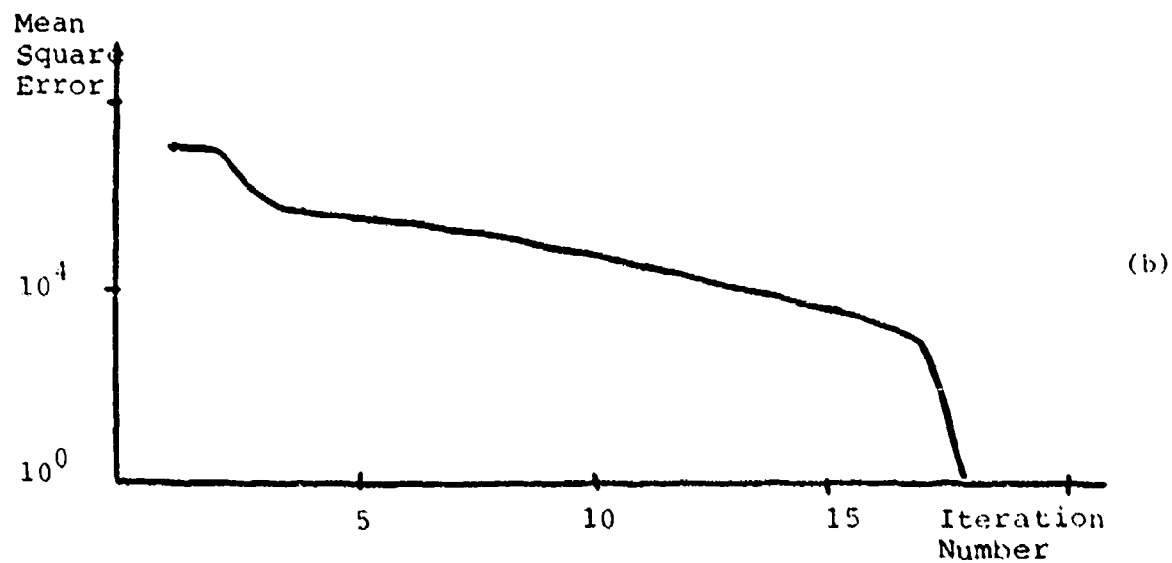
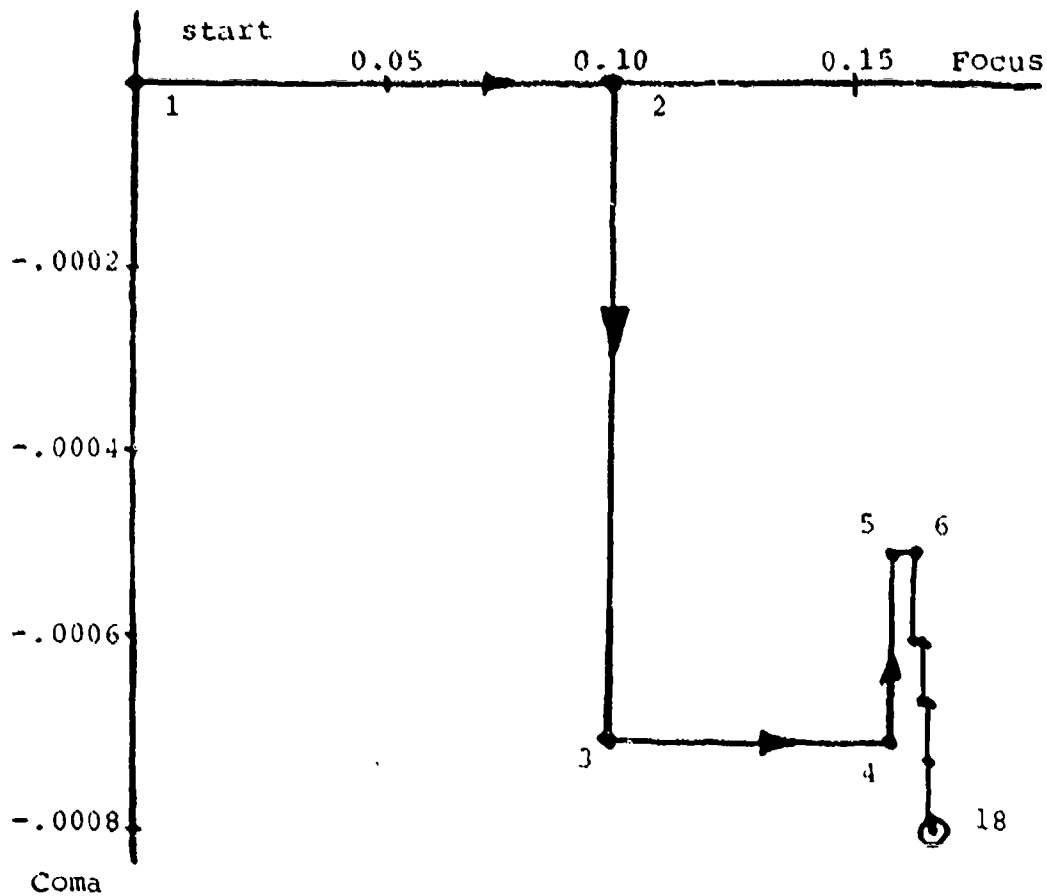


Figure 11. (a) Search path in focus-coma space and (b) the corresponding MSE.

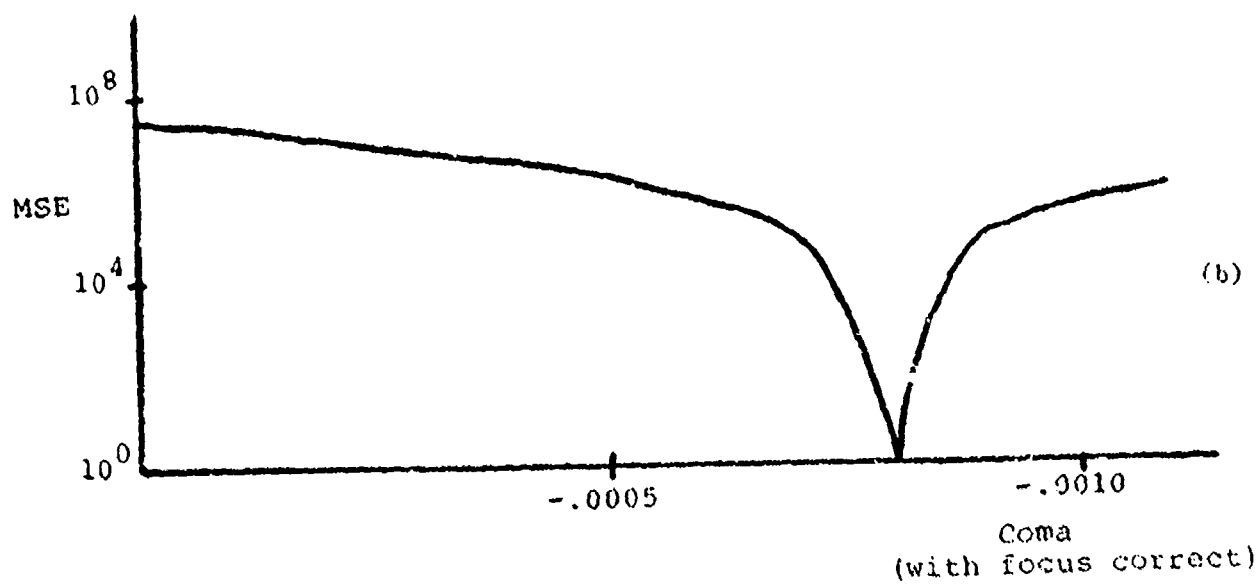
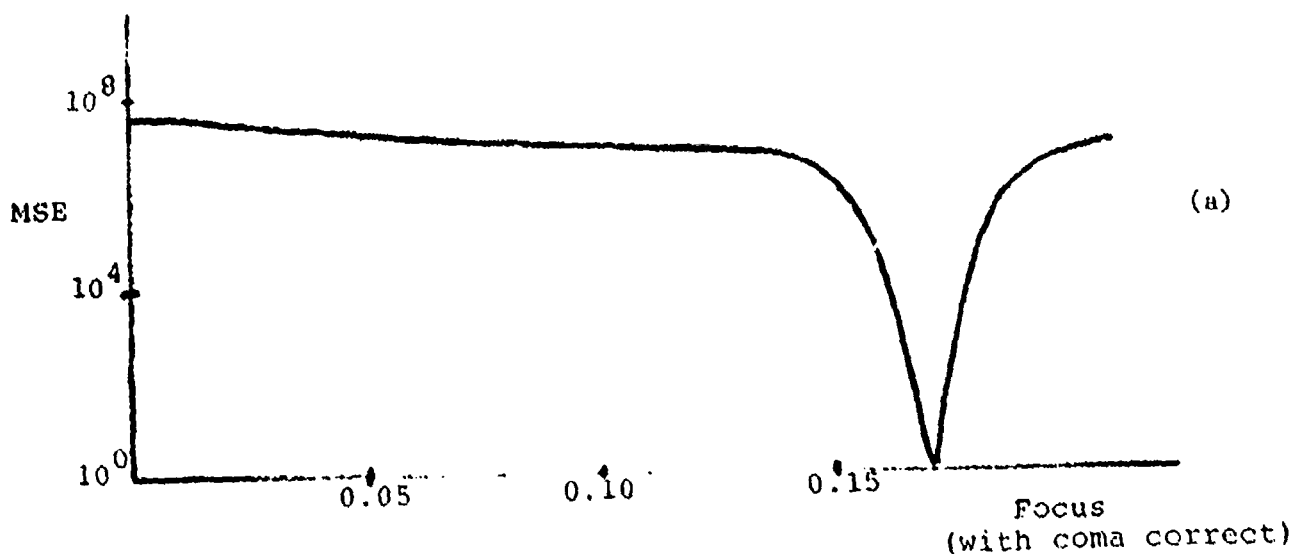


Figure 12. MSE search metric (a) vs. focus and (b) vs. coma.

2.5 Discussion.

These results are quite promising, except that they are only computer simulations. Also they are all results for one-dimensional signals.

We would, next, apply the algorithm to simulated data in two dimensions. Reference [3] shows some results that are applicable. Notably, in [3] the authors found that the metric had to be modified to find, first, a minimum when only low-order (frequency) components of the unknown object were to be estimated.

A further step would be to attempt an experimental verification of the theory. This would be done, first, in a lab and under a controlled environment, where $w_1(f)$ would be determined by an auxiliary method to test how well the technique works.

Then the technique would be tried on an adaptive optics system in which two simultaneous measurements can be made. A natural place to try the method would be on an astronomical telescope, perhaps at Mauii.

3. Recognition

3.1 General

A particularly challenging and difficult problem is the automatic recognition of an object in a real scene. Successful solutions to the problem have depended in great part on the nature of the object and the environment of the observation/detection process.

Perhaps the most successful application of automatic recognition is the bar code scanner. Here the system engineer needs only to detect a series of on-off pulses from a bar code which has been physically placed on the object. The measurement system is a relatively noise-free environment provided by a scanning laser beam which penetrates a small window.

Another successful application is a character reader. Typically one feeds a page into an optical scanner, then the information is digitized, stored and processed to recognize lines of characters and the characters, themselves. Again the object is highly structured (except for handwritten material, which is a far more difficult problem) and the measurement environment is relatively benign.

Industrial inspection is another successful application. For example, the U.S. Treasury Department inspects all printed money by comparing each note (in a large page of notes) to a

standard note. The pages fly off the press at such a speed that automatic detection of flaws is the only reliable way to find them. Again, the detection is done by digitizing an image of the note and by digital correlation with the standard.

In all of these applications, a common thread is the digitization of the object and computer processing to make decisions. For objects and scenes which are less standardized, the computer processing needs are overwhelming. A partial solution is provided by optical signal processing which uses the massive, parallel computing power of lenses and masks to cross-correlate the image of an object with the image of the scene.

A good summary of the literature on optical processing appears in a special issue of Optical Engineering, Reference [4]. This issue reviews Vander Lugt filters, phase-only filters, techniques to handle rotation and scale variations, synthetic discriminant functions, Wigner distributions and other specialized techniques. We are especially interested in the work on phase-only filtering [5] [6] [7] because of our earlier work [8] [9] [10] which uses interactive techniques to design holographic and phase-only filters.

3.2 Optical Processing

It is well known that if a real object $o(x)$ is to be detected in a real scene $s(x)$, the crosscorrelation of $o(x)$ with $s(x)$ is an optimal statistic for detection. The most likely location of the object is where $c(x)$, the crosscorrelation, is a maximum.

In the spatial domain $c(x)$ is

$$c(x) = \int s(u) o(u-x) du = s(x) * o(-x) ; \quad (9)$$

and in the spatial frequency domain $C(f)$ is

$$C(f) = S(f) O^*(f). \quad (10)$$

To see why crosscorrelation is a sensible statistic for detection of an object, consider a scene consisting of the object plus noise.

$$s(x) = o(x) + n(x). \quad (11)$$

The noise $n(x)$ could be measurement noise or extraneous objects. Then $C(f)$ is

$$C(f) = [O(f) + N(f)] O^*(f) = |O(f)| + N(f) O^*(f). \quad (12)$$

With $o(x)$ located at $x=0$, we expect $c(x)$ to be maximum at $x=0$.

But

$$\begin{aligned} c(0) &= \int c(f) df \\ &= \int |o(f)|^2 df + \int N(f) o^*(f) df. \end{aligned} \quad (13)$$

The first term is the signal energy in $o(x)$, a real non-negative quantity. The second term is noise-like, whose mean tends to zero and whose variance is complicated to compute. However, the detectability of the object is strongly dependent on the signal energy term.

The crosscorrelation in (9) can be computed optically. A typical processor consists of two lenses and a mask. The first lens calculates the Fourier transform of the scene, the mask forms the product in (10), and the second lens takes the inverse Fourier transform to form $c(x)$.

Two important elements of this scheme are the mask and the transducer that forms the optical scene. We will not attempt to catalogue the transducer solutions. A typical approach is to capture the scene with a video camera and to display the scene on a semi-transparent medium which can be, simultaneously, probed by a collimated, monochromatic light source. This will form an optical signal which can be transformed by a lens.

We are especially interested in the mask. The choice of a suitable mask has a 100-year history. Early attempts by E. Abbe in 1893 and by A. B. Porter in 1906 are reviewed in [11]. They used aperture stops to provide a gross spatial filtering of a scene. Goodman [11] also describes work done in the 1950's by A. Marechal, who used an amplitude and binary phase filter to restore a focus-degraded image.

In 1964, A. Vander Lugt [12] described an optical filtering method that detects a general object in a scene. He used a holographic technique to record the object's Fourier transform, which is the mask required by the optimal filter. The mask attenuates the optical intensity in the Fourier transform domain with attenuations which vary continuously over the range 0 to 1. The desired crosscorrelation appears in an off-axis term in the back focal plane of the second lens.

One problem with the holographic approach of Vander Lugt is that the continuous, 0 to 1 attenuation of the mask is difficult to achieve since there are usually some non-linearities in the fabrication process. Another problem is that a large portion of the energy at the output of the optical processor is wasted since the desired crosscorrelation appears off-axis. The largest energy is on-axis and an amount equal to the the desired signal appears in symmetry to it.

The second problem is eliminated if a phase mask can be made [5]. All the signal energy will appear in an on-axis, crosscorrelation term. Also, the first problem will be reduced if the phase is binary [7]. In the next section we show some examples. References [4] through [7] give a good review of the literature.

3.3 Example

In our examples we define the observable function $CCF(x)$, which is the magnitude squared of the crosscorrelation function of $s(x)$ with $o(x)$. We further normalize $CCF(x)$ so that its maximum value is unity. Thus

$$CCF(x) = |c(x)|^2 / B , \quad (14)$$

where B is the maximum value of $|c(x)|^2$.

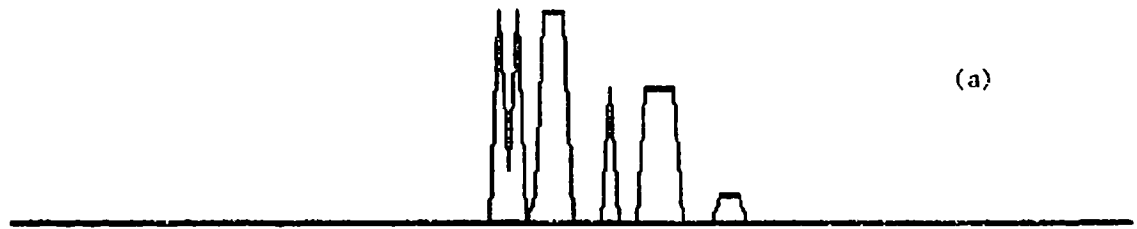
In Figure 13 we show an object $o(x)$ and a scene $s(x)$. The scene has object and noise in it.

Figure 14 shows $CCF(x)$ for several filters, $H(f)$, which are used to perform the crosscorrelation. In all cases the frequency crosscorrelation is

$$C(f) = S(f) H(f) . \quad (15)$$

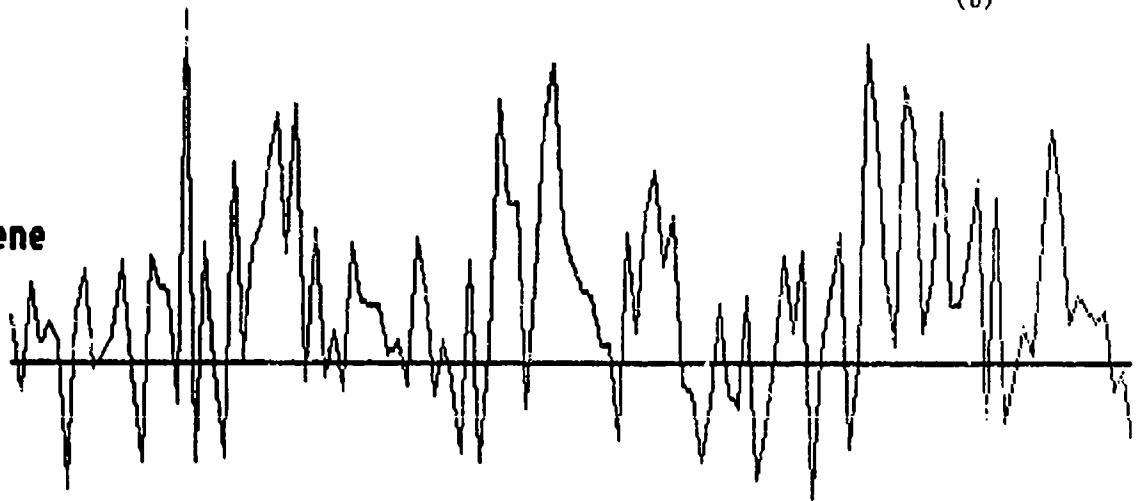
In Figure 14(a), $H(f)$ is $O^*(f)$, the conventional matched filter. $H(f)$ is a complex-valued filter, realized by whatever means. As expected the peak of $CCF(x)$ appears at the location of the input object.

object



(a)

noisy scene



(b)

Figure 13. (a) Object to be found in (b) the noisy scene.

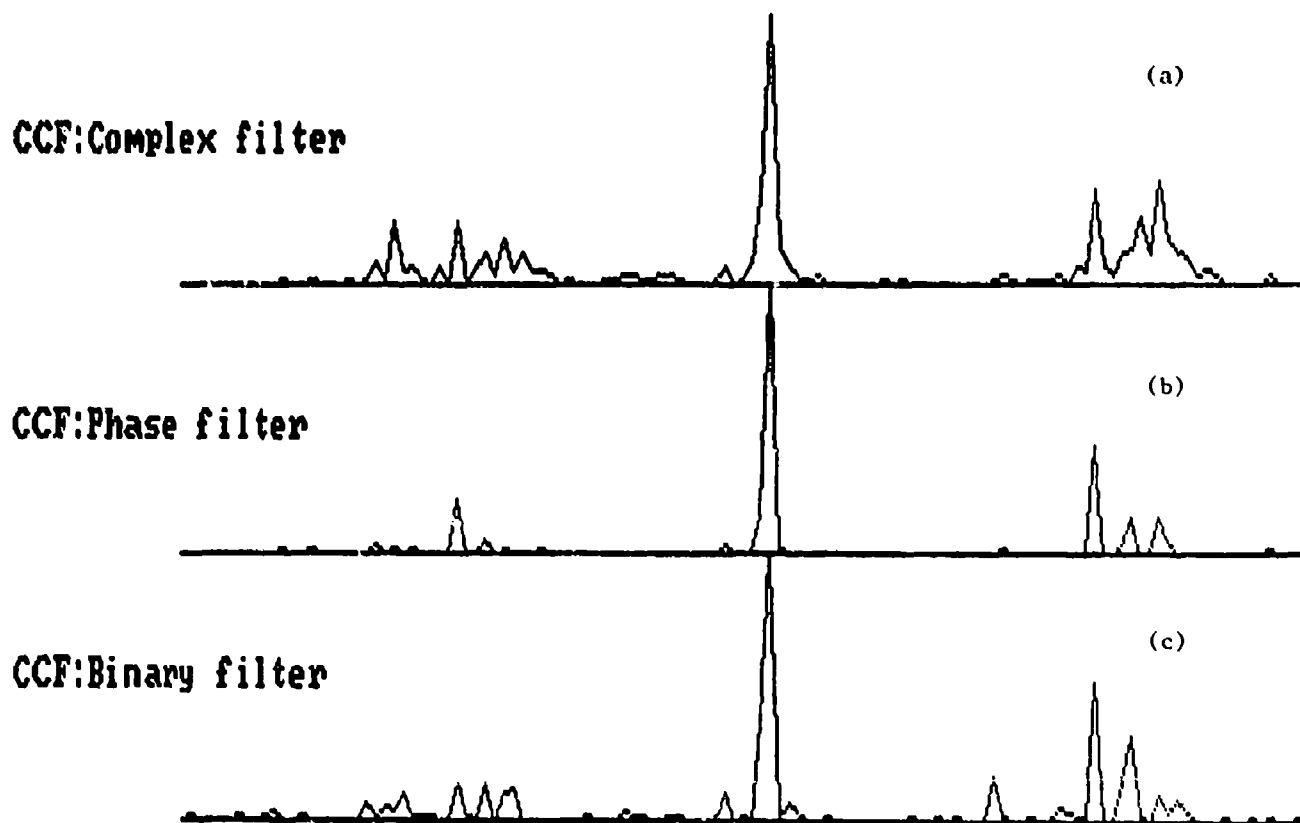


Figure 14. Crosscorrelation of the scene and object for various object filters, $H(f)$.

(a) $H(f) = \text{matched filter} = o^*(f)$.

(b) $H(f) = \text{phase-only filter} = o^*(f) / |o(f)|$.

(c) $H(f) = \text{binary filter} = \text{Sign} (\text{Real} (o^*(f) e^{jt}))$

Figure 14(b) shows CCF(x) when the H(f) is a phase-only filter, namely the phase of $O^*(f)$. That is,

$$H(f) = O^*(f) / |O(f)| \quad . \quad (16)$$

Note that the peak is better defined when compared with Figure 14(a). This is a typical result for a phase-only filter, when the object has many edge-like features. Equation (16) has the effect of enhancing the high-frequency region of $C(f)$ which, for a signal with large high-frequency content, sharpens the crosscorrelation function.

Figure 14(c) shows CCF(x) when the filter is a binary version of $O^*(f)$. Thus, H(f) is

$$H(f) = \begin{cases} 1 & , \quad \text{Re} \{ O^*(f) e^{-jt} \} \geq 0 \\ -1 & , \quad \text{Re} \{ O^*(f) e^{-jt} \} < 0 \end{cases} \quad . \quad (17)$$

In Equation (17), t is a rotation angle to be described later. Note that there is only a slight degradation between 14(b) and 14(c); this, in spite of the fact that H(f) is binary with implications for ease of fabrication.

3.4 Phase Rotation

To calculate $CCF(x)$ in Figure 14(c) we rotated the phase of $O^*(f)$ before we binarized it. This was our rationale: First we binarized the real part of $O^*(f)$ and found $CCF(x)$. Then we binarized the imaginary part of $O^*(f)$ and found $CCF(x)$. The results were different. This led us to examine $CCF(x)$ as a function of the rotation angle.

There seemed to be a particular angle, 30 degrees in this case, where the peak was best defined. Figure (15) shows $CCF(x)$ for three of the angles: 0, 30 and 90 degrees. Arguably, the second CCF in Figure 15 is the best formed.

To choose the best angle we start with a noiseless scene and define a metric, M , as follows:

$$M = 1 / (\sum CCF(k) - 1) , \quad (18)$$

where $CCF(k)$ is the discrete form of $CCF(x)$. For a noiseless scene we expect that $CCF(k)$ will be unity at $k = 0$, representing the energy in the object. All other non-zero values of $CCF(k)$ represent noise, sometimes called clutter. Thus the sum of $CCF(k)$, less 1, will be a measure of the total clutter energy. This implies that M is a signal-to-clutter ratio.

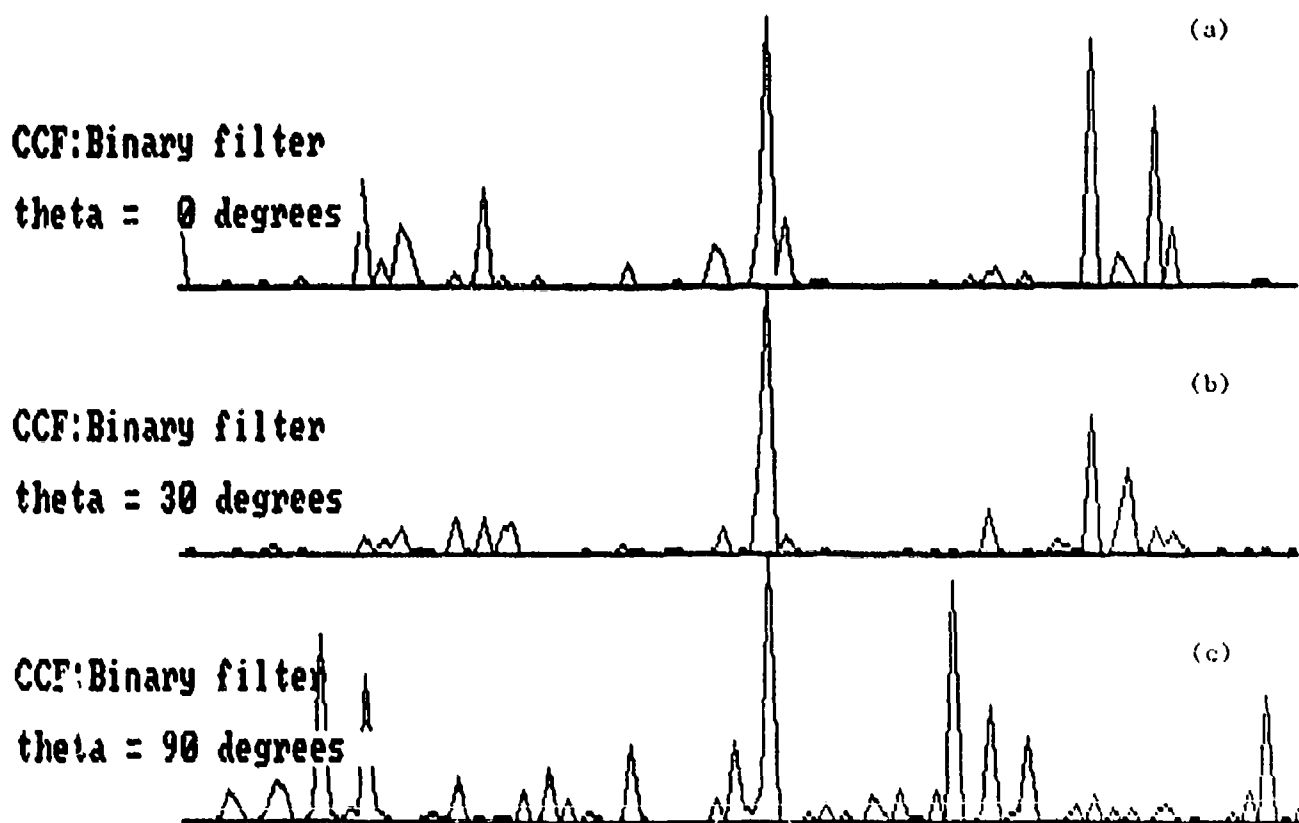


Figure 15. Crosscorrelation for various phase-rotated binary filters.
(a) $t = 0$, (b) $t = \pi/6$, (c) $t = \pi/2$.

In Figure 16 we show M for angles 0 to 90 degrees. (The extended curve is symmetric about both 0 and 90 degrees.) It peaks, somewhat weakly, at 30 degrees.

In Figure 17 we show the CCF plots for a noiseless scene and for binarization angles of 0, 30, and 90 degrees. Indeed, the 30-degree plot does have the best shape (lowest sidelobes), although the difference is not dramatic.

In Figures 18, 19 and 20 we show another example. The object and noisy scene are in Figure 18. The CCF's for three kinds of $H(f)$ are shown in Figure 19. The binary phase-only CCF in Figure 19(c) is that for the 30 degree rotation angle. And in Figure 20 we show the CCF's for three rotation angles.

Note that the 90-degree CCF in Figure 20(c) is better than that for 30 degrees. This is a typical result for noisy data and led us to try averaging the CCF over the binarizing angle.

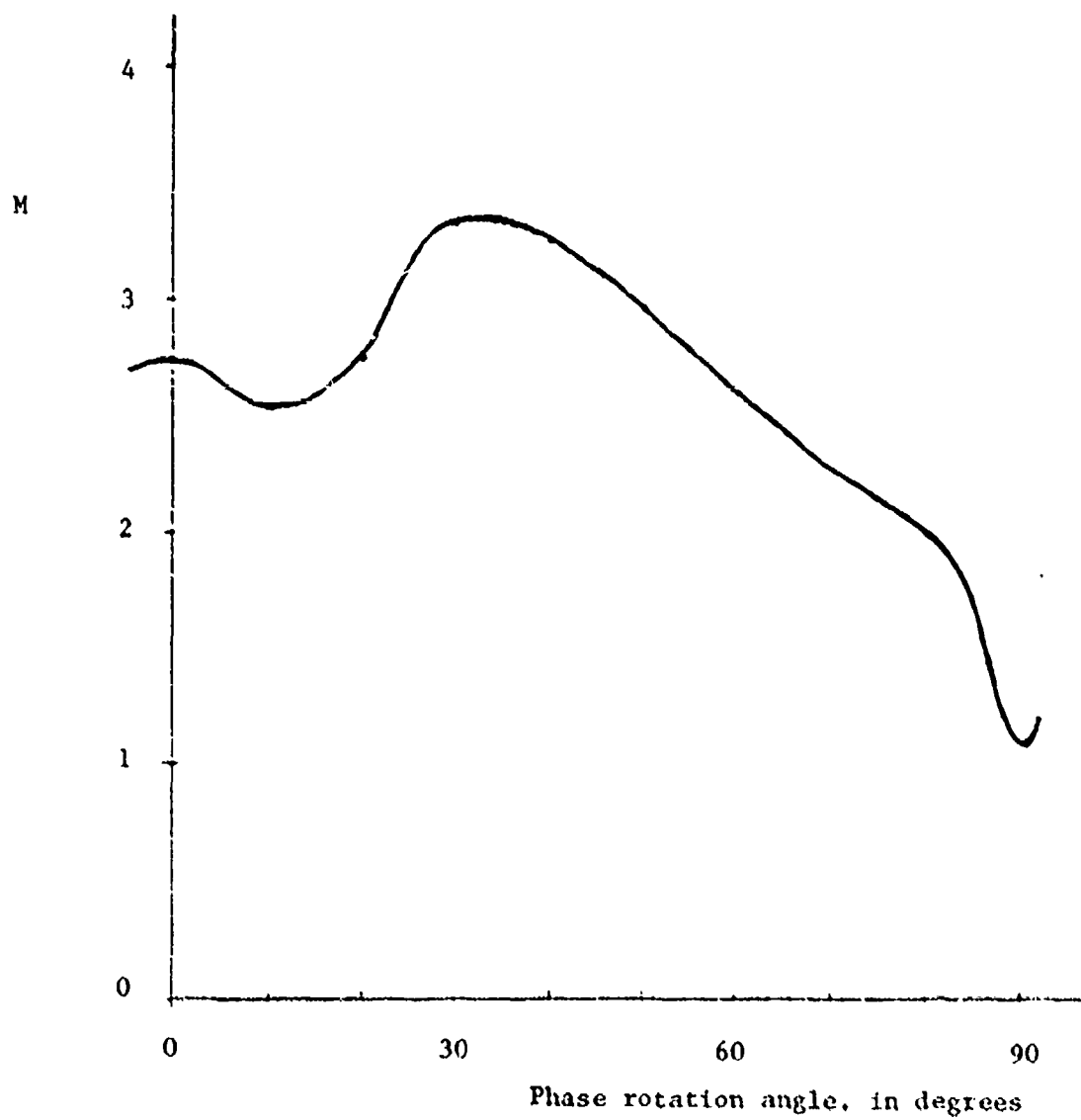


Figure 16. Signal-to-clutter ratio, M , vs. angle.
(The plot is symmetric about both 0 and 90 degrees.)

CCF:Binary filter

theta = 0 degrees

(a)

CCF:Binary filter

theta = 30 degrees

(b)

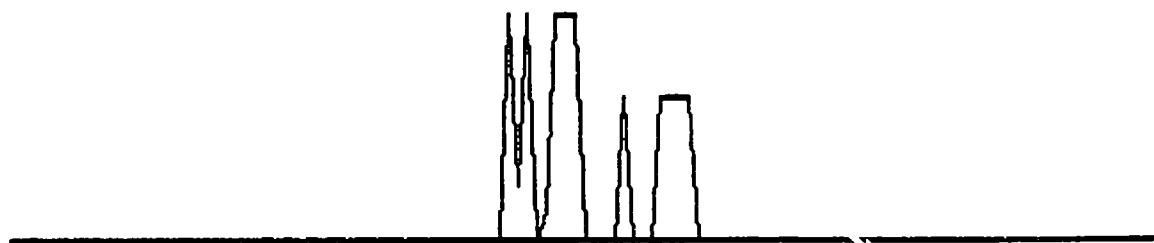
CCF:Binary filter

theta = 90 degrees

(c)

Figure 17. Noiseless CCF's for angles of 0, 30 and 90 degrees.

object



noisy scene

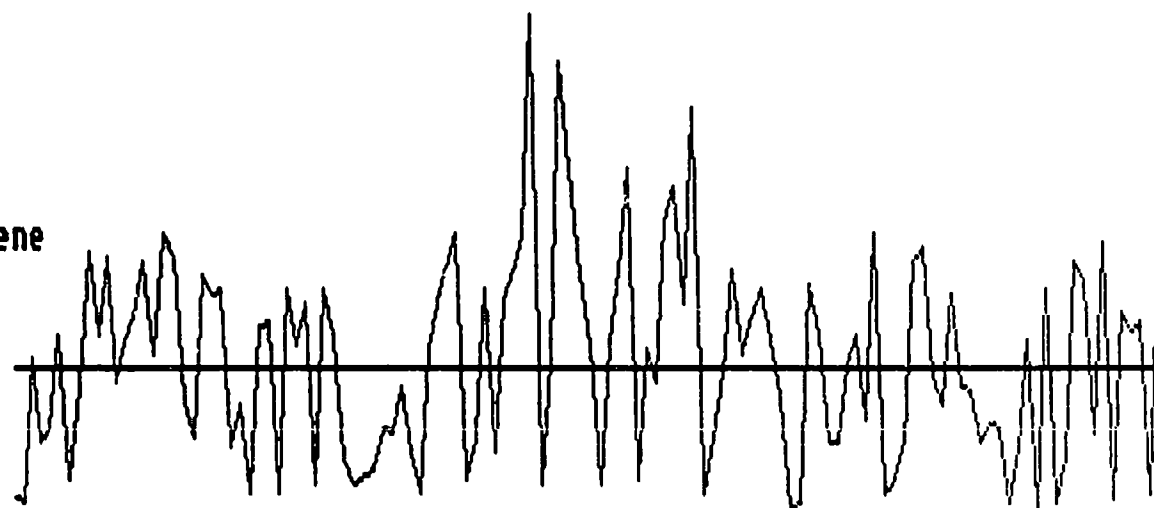


Figure 18. Another example of object and noisy scene.

CCF:Complex filter

(a)

CCF:Phase filter

(b)

CCF:Binary filter

(c)

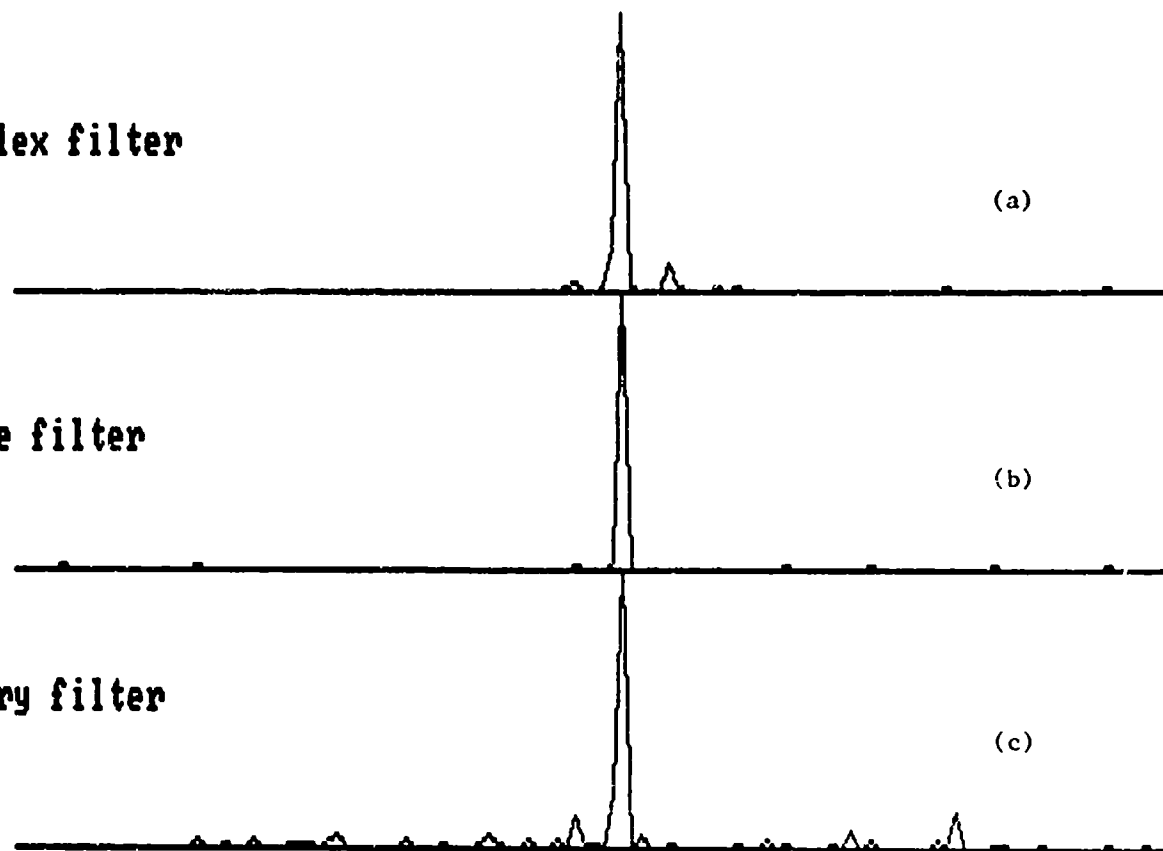
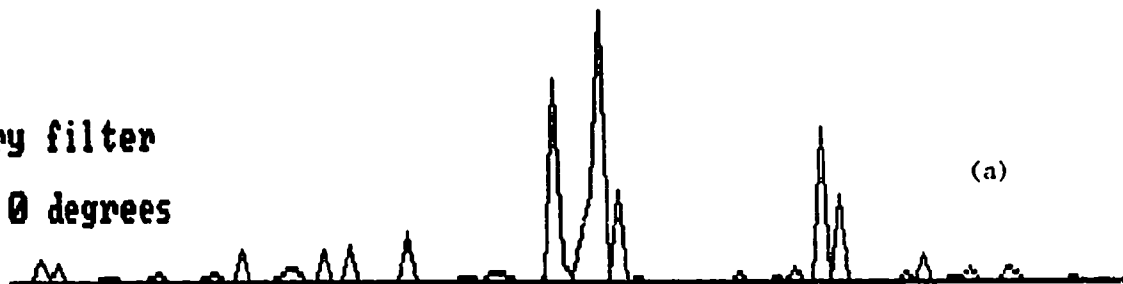


Figure 19. CCF's for various filters, scene of Figure 18.

CCF:Binary filter

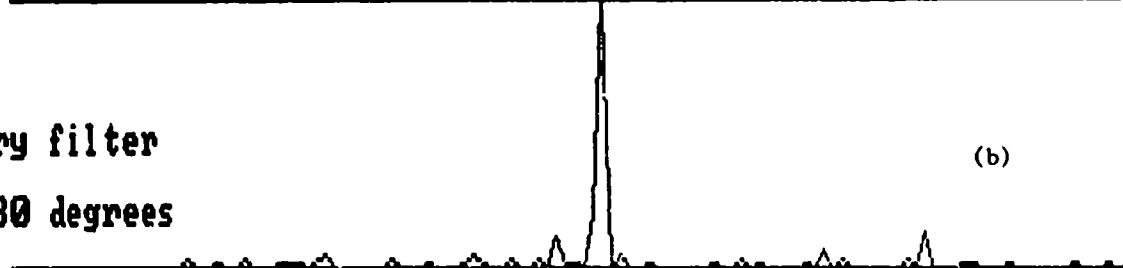
theta = 0 degrees



(a)

CCF:Binary filter

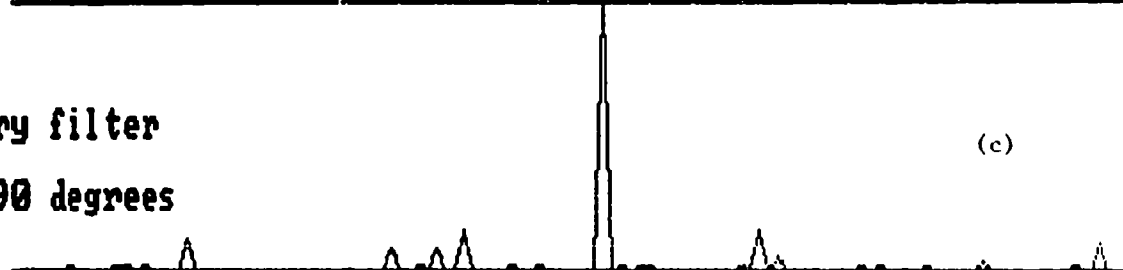
theta = 30 degrees



(b)

CCF:Binary filter

theta = 90 degrees



(c)

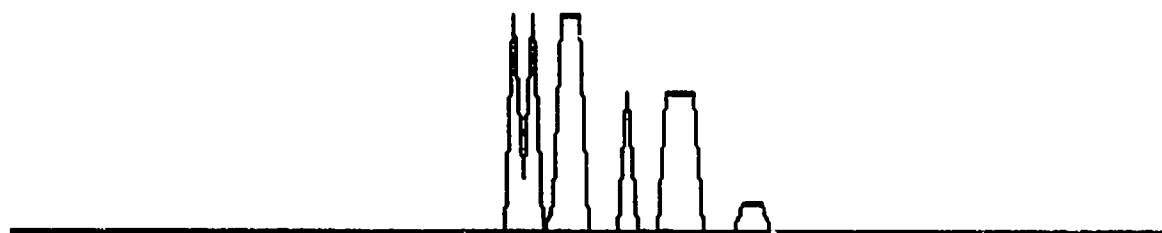
Figure 20.

CCF's for various phase-rotated binary filters.
(The 30-degree-filter CCF is also shown in Figure 19(c)
although the 90-degree CCF is the cleanest.)

Our final example is shown in Figures 21, 22 and 23. The "CCF:Binary filter" plot in Figure 22(c) was calculated by averaging 10 CCF's for binarizing angles from 0 to 90 degrees. It is a good compromise between the matched filter result in Figure 22(a) and the phase-only filter result in Figure 22(b).

The individual CCF's for 0, 30 and 90 degrees are shown in Figure 23. Significantly, each is inferior to the average, which is shown in Figure 22(c). This result was quite consistent for other noise realizations.

object



noisy scene

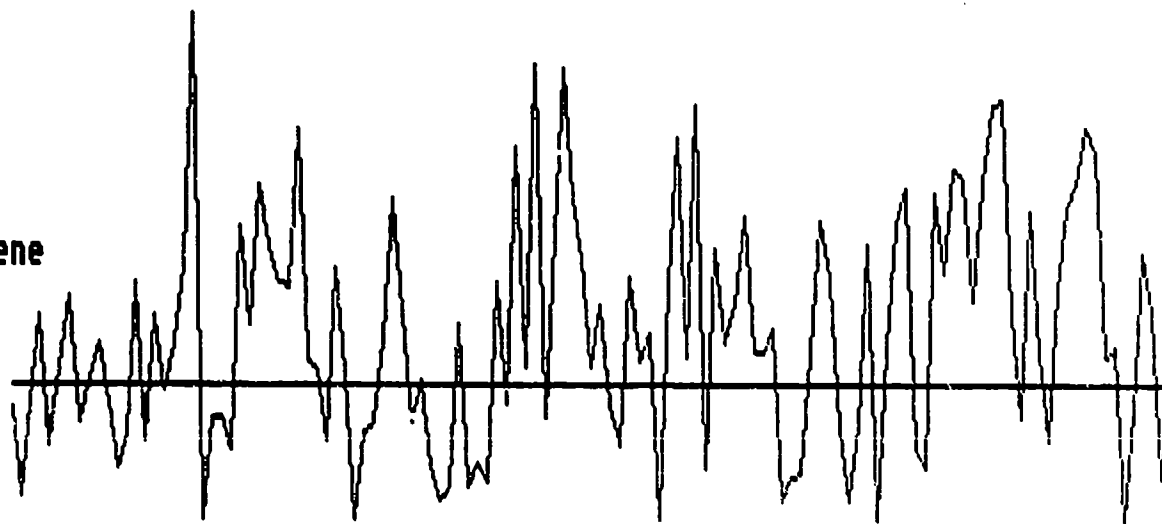


Figure 21. Final example.

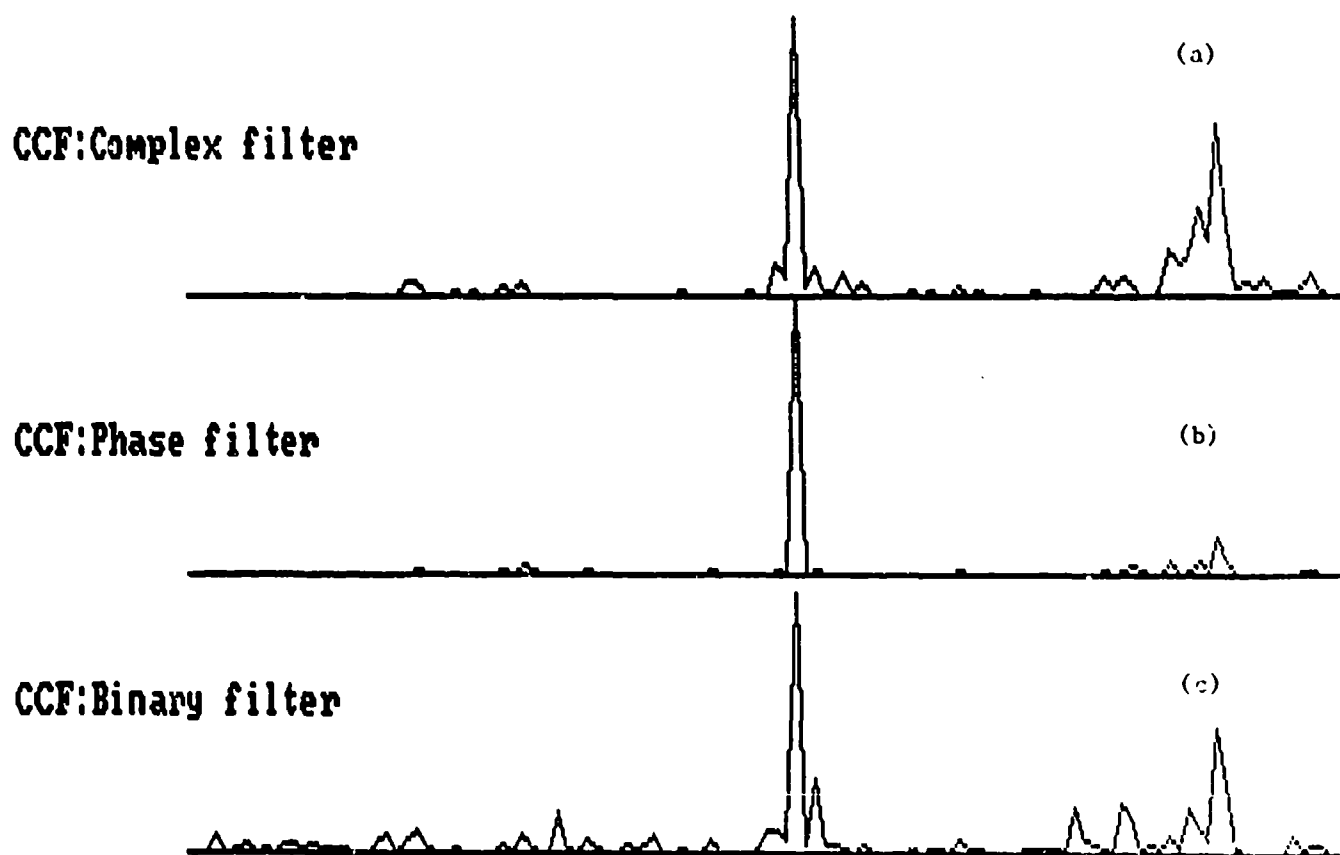
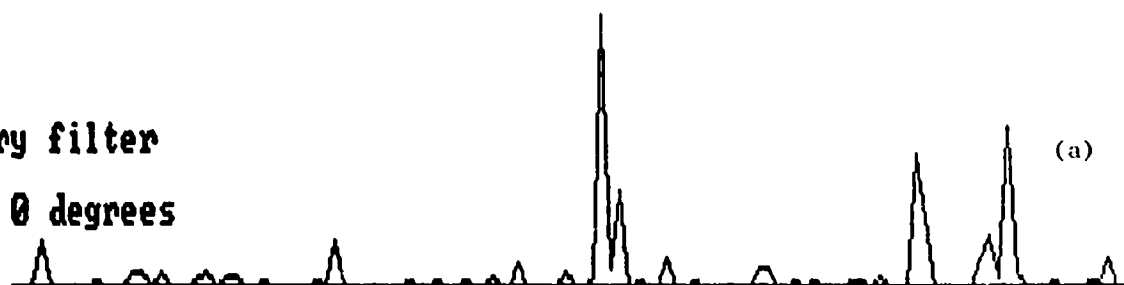


Figure 22. CCF's for various filters, scene of Figure 21.
The binary filter is an average, as explained in the text.

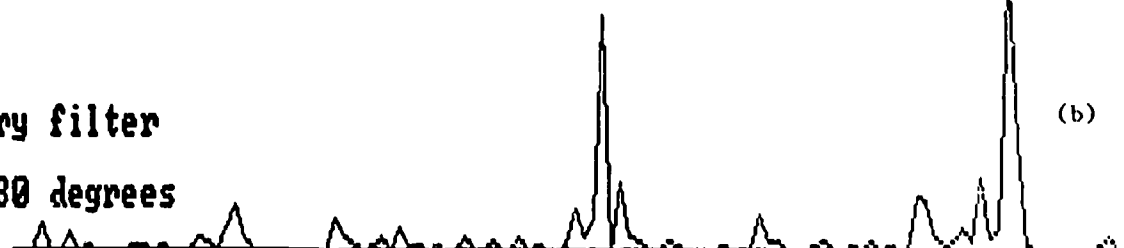
CCF:Binary filter

theta = 0 degrees



CCF:Binary filter

theta = 30 degrees



CCF:Binary filter

theta = 90 degrees

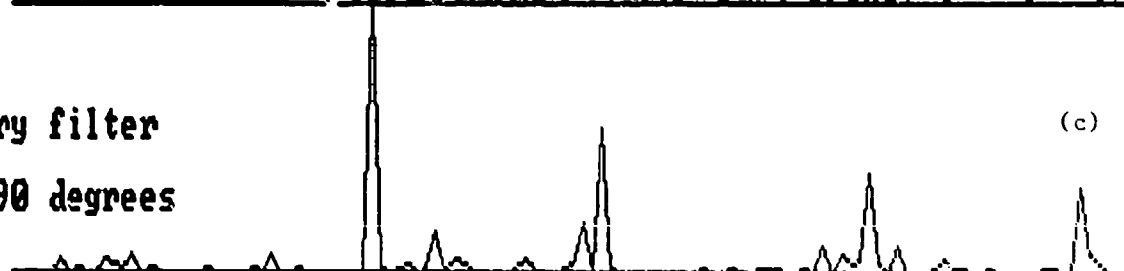


Figure 23. CCF's for various phase-rotated binary filters.
(The average of 10 such results is shown in Figure 22(c).
Note that Figure 22(c) is cleaner than any of these.)

3.5 Discussion

We have made some very modest attempts to understand and to model the binary phase-only filtering technique. We find that the phase-only filter can be advantageously rotated before the binarization process. However it is difficult to predict, in the face of noisy data, which angle produces the best crosscorrelation.

An average-over-angle technique is introduced. This approach is like the classical minimax (minimize the maximum error) approach to detection of a signal with random phase - a solution that requires an assumption of uniformly distributed, random phases and gives rise to in-phase (0 degree) and quadrature (90 degree) detection.

These examples and observations lead to several questions:

1. Does the averaging of binary phase-only filtered CCF's have a theoretical basis?
2. Do these results/observations extent to imaging in two dimensions?
3. What is the expected performance?
4. How would an optical system achieve the averaging?
5. Would averaging over just two angles, say 0° and 90° , be a good approach?

These are questions that are left to further study.

References

1. R.A. Gonsalves, "Phase Retrieval from Modulus Data," J. Opt. Soc. Am., Vol. 66 (1976), p. 961.
2. R.A. Gonsalves, "Phase Retrieval and Diversity in Adaptive Optics," Optical Engineering, Vol. 21, No. 5, (1982) p. 829.
3. R.G. Paxman and J.R. Fienup, "Optical Missalignment Sensing and Image Reconstruction using Phase Diversity," J. Opt. Soc. Am., Vol. 5, No. 6, (1988) p. 914.
4. J.L. Horner, Guest Editor for "Optical Pattern Recognition," Optical Engineering, Vol. 23, No. 6. (1984).
5. J.L. Horner and P.D. Ginaino, "Phase-Only Matched Filtering," Appl. Opt., Vol. 23, (1984) p. 812.
6. J.L. Horner and P.D. Ginaino, "Additional Properties of the Phase-Only Correlation Filter," Optical Engineering, Vol. 23, No. 6, (1984) p. 695.
7. H. Bartelt and J. Horner, "Improving binary phase correlation filters using iterative techniques," Appl. Opt., Vol. 24, (1985) p. 2894.
8. R. Gonsalves, R. Dumais and P. Considine, "On Optimal Holographic Filters," Proc. SPIE, Vol. 45, (1974) p. 293.
9. R. Gonsalves and R. Dumais, "Spatial Filtering with Amplitude-Distorted VanderLugt Filters," Optical Engineering, Vol. 12, No. 2, (1973), p. 43.
10. R. Gonsalves and P. Considine, "Spot Shaping and Incoherent Optical Smoothing for Raster Scanned Imagery," Optical Engineering, Vol. 15, No. 1, (1976) p. 64.
11. J.W. Goodman, Introduction to Fourier Optics. McGrawHill, N.Y. (1968).
12. A.B. Vander Lugt, " IEEE Trans. Inform. Theory. IT-10, No.2 (1964).



MISSION of Rome Air Development Center

RADC plans and executes research, development, test and selected acquisition programs in support of Command, Control, Communications and Intelligence (C³I) activities. Technical and engineering support within areas of competence is provided to ESD Program Offices (POs) and other ESD elements to perform effective acquisition of C³I systems. The areas of technical competence include communications, command and control, battle management information processing, surveillance sensors, intelligence data collection and handling, solid state sciences, electromagnetics, and propagation, and electronic reliability/maintainability and compatibility.